Attenuation of Inlet Flow Distortion Upstream of Axial Flow Compressors

G. M. CALLAHAN*
Pratt & Whitney Aircraft, West Palm Beach, Fla.

AND

A. H. STENNING†
Lehigh University, Bethlehem, Pa.

A linearized analysis predicts the velocity and static pressure redistribution in a distorted flowfield upstream of a low hub-tip ratio axial flow compressor as a function of the slope of the compressor pressure rise vs mass flow rate characteristic. The attenuation of axial velocity distortion and the magnitude of the generated circumferential and radial velocities are found to increase with a steeper negative slope of the compressor characteristic. Analytical results indicate that the magnitude of the upstream flow redistribution is approximately halved when radial velocities are conserved within the compressor as compared to the results assuming that radial velocities are suppressed within the compressor. The test compressor suppressed internal radial velocities and data verified the appropriate analysis. The local slope of the distorted characteristic was found to be significantly less than the undistorted slope. Much of the difference between the local distorted slope and the undistorted compressor characteristic slope was attributable to rotor unsteady effects.

Nomenclature

$A_{m,n}$ = series coefficient of upstream potential function
a = local speed of sound
g_c = Newton's law constant
J_n = Bessel function of the first kind, order n
$K_{m,n}$ = proportionality constant
M = local Mach number
p = pressure
R = linear combination of Bessel functions of the first and second kind
r = radial coordinate, generally normalized with respect to the tip radius
S_1 = static pressure-rise parameter
U = total axial velocity
u = perturbation axial velocity
V = total cross-flow velocity
v = perturbation cross-flow velocity
W = total radial velocity
w = perturbation radial velocity
x = axial distance, generally normalized with respect to the tip radius
x_c = axial distance parameter equal to $x/(1 - M^2)^{1/2}$
Y_n = Bessel function of the second kind, order n
γ = hub-tip ratio of compressor
ϵ_n = Fourier coefficient for input distortion
θ = circumferential coordinate
$\lambda_{m,n}$ = eigenvalue in cylindrical analysis
ρ = density
ϕ = velocity potential function

Subscripts

m = radial harmonic number
n = circumferential harmonic number
$-\infty$ = far upstream of the compressor
0_- = compressor face
0_+ = compressor exit
$+\infty$ = far downstream of the compressor
$+$ = downstream
$-$ = upstream

Presented as Paper 69-485 at the AIAA 5th Propulsion Joint Specialist Conference, U.S. Air Force Academy, Colorado, June 9–13, 1969; submitted June 16, 1969; revision received November 10, 1969.

* Assistant Project Engineer, Systems Analysis Department.
† Professor of Mechanical Engineering. Associate Fellow AIAA.

Introduction

As part of an aircraft turbojet engine, an axial flow compressor must operate at off-design conditions. One important off-design condition encountered is operation with an inlet total pressure distortion generated by inlet ducting upstream of a compressor. This paper studies the flow redistribution upstream of low hub-tip ratio compressors with a total pressure distortion of the flow originating far upstream.

Significant experimental and analytical work has been published on the effect of total pressure distortions on the performance of axial compressors and the attenuation of inlet distortions within the compressors. Dunham[1,5] presented an extensive bibliography of the published material concerning inlet total pressure distortions within axial flow compressors. Pearson and McKenzie[2] noted that when a total pressure distortion with a uniform static pressure was introduced far upstream of an axial flow compressor, a flow redistribution occurred upstream because of the presence of the compressor, and the static pressure profile changed as the flow approached the compressor face. Plourde and Stenning[3] analyzed the two-dimensional flowfield upstream, within, and downstream of a high hub-tip ratio compressor with a circumferential total pressure distortion introduced far upstream. A thorough study of the three-dimensional flowfield upstream of a low hub-tip ratio compressor operating with a total pressure distortion imposed on the flow far upstream has not, to date, been accomplished. It is the intent of this paper to report such a study.

Plourde and Stenning found in their upstream analysis that the flow redistribution was dependent upon the slope of the pressure-rise vs mass flow rate characteristic of the compressor. In low hub-tip ratio compressors the pressure-rise characteristic can vary from root to tip along the blades and the inlet distortion may vary in the radial as well as the circumferential direction at its origin. An analysis of the flowfield had to account for these three-dimensional effects.

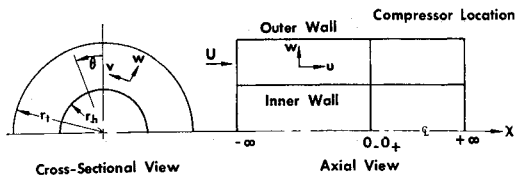

Fig. 1a) Cylindrical coordinate system.

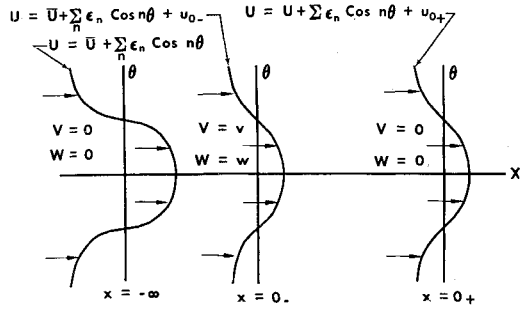

Fig. 1b) Velocity field for "long" compressor analysis.

It was also desired to obtain an approximation to the inlet Mach number effect on the upstream flow redistribution.

The analysis developed in this paper assumes the inlet total pressure distortion to be a small perturbation superposed on the main flow. The static pressure is assumed uniform at the distortion origin, hence, the inlet distortion is a distortion in the incoming axial velocity profile. The flow is affected by the compressor and axial, radial, and circumferential velocity components are developed as the flow approaches the compressor. The analysis is developed to predict the velocity components generated by the flow redistribution.

In the analysis of the upstream distorted flowfield, and the effect the compressor has on it, certain assumptions had to be made regarding the static pressure at the compressor exit. Two compressor exit conditions were of interest: 1) a uniform exit static pressure profile, herein defining a "long" compressor and 2) a nonuniform exit static pressure profile, defining a "short" compressor. In a "long" compressor, radial pressure gradients within the compressor act over a sufficient axial distance to remove the radial velocities entering the compressor, and the flow leaves the last stator row with zero radial and tangential velocities, hence, the compressor exit static pressure is constant and no further flow redistribution occurs. For a "short" compressor, radial velocities that exist at the compressor face are conserved within the compressor and appear at the compressor exit, hence, the exit static pressure is necessarily nonuniform and flow redistribution occurs both upstream and downstream of the compressor. Most multistage compressors and low aspect ratio (<2) single-stage fans fall into the category of "long" compressors. Single-stage fans of high aspect ratio (>2) can fall into the category of "short" compressors.

An experimental program was developed to verify the analytical results because no previous experimental work has been found that measures the velocity and pressure profiles upstream of a low hub-tip ratio axial flow compressor with a total pressure distortion originating far upstream (a reasonable distance satisfying the far upstream condition was found to be at least two compressor tip radii before the compressor). Most of the inlet distortion experimental work has dealt with the performance of the compressor or with distortion attenuation and blade forces within the compressor. Total pressure distortions were usually generated with screening located directly before the compressor face. Robbins and Glaser[4] conducted performance tests on a low hub-tip ratio compressor with a distortion originating approximately 1.25 compressor radii upstream of the compressor face. They measured the velocity and pressure profiles at the compressor face but sufficient information as to the upstream amplitude of the distortion and the compressor pressure-rise characteristic was not presented to obtain a quantitative comparison with the analysis developed herein. An analysis of the flow redistribution upstream of a "long" compressor and comparison with test data using a 360° cosine wave inlet distortion profile follows.

Analysis—"Long" Compressor

A circular cylindrical coordinate system is used to describe the inlet, compressor, and exit configuration and is shown in Fig. 1a. The fluid occupies an annular region extending from $x = -\infty$ to $x = +\infty$ with the compressor being assumed a thin disk located at $x = 0$.

A total pressure distortion is imposed at $x = -\infty$, where the static pressure is assumed constant, resulting in a distortion in the incoming axial velocity. At any point in the upstream flowfield, the velocity and corresponding density and pressure distributions can be expressed by

$$U = \bar{U} + \sum_n \epsilon_n \cos n\theta + u$$
$$V = v,\ W = w,\ \rho' = \bar{\rho} + \rho,\ p' = \bar{p} + p \tag{1}$$

The symbols U, V, and W represent the axial, circumferential, and radial velocities, respectively. $\bar{U}$ is the mean undistorted axial velocity and

$$\sum_n \epsilon_n \cos n\theta$$

is a small ($\epsilon_n \ll \bar{U}$) velocity superposed on $\bar{U}$ at $x = -\infty$. In general, ϵ_n is a function of the radius. The subscript n is the circumferential wave number. The density and pressure at any point is expressed by ρ' and p' with their mean values being $\bar{\rho}$ and $\bar{p}$, respectively. The symbols u, v, w, ρ, and p represent the perturbation terms of velocity, density, and pressure that are generated in the upstream flowfield ($-\infty \leq x \leq 0$) because of the presence of the compressor. All perturbation terms are assumed zero at $x = -\infty$. The velocity distribution is shown in Fig. 1b.

The inviscid flow momentum equations in circular cylindrical coordinates are

$$W\frac{\partial W}{\partial r} + \frac{V}{r}\frac{\partial W}{\partial \theta} + U\frac{\partial W}{\partial x} - \frac{V^2}{r} = \frac{1}{\rho'}\frac{\partial p'}{\partial r} \tag{2}$$

$$W\frac{\partial V}{\partial r} + \frac{V}{r}\frac{\partial V}{\partial \theta} + U\frac{\partial V}{\partial x} + \frac{WV}{r} = -\frac{1}{\rho' r}\frac{\partial p'}{\partial \theta} \tag{3}$$

$$W\frac{\partial U}{\partial r} + \frac{V}{r}\frac{\partial U}{\partial \theta} + U\frac{\partial U}{\partial x} = -\frac{1}{\rho'}\frac{\partial p'}{\partial x} \tag{4}$$

The continuity equation for compressible flow is

$$\frac{\partial(\rho' r W)}{\partial r} + \frac{1}{r}\frac{\partial}{\partial \theta}(\rho' r V) + \frac{\partial}{\partial x}(\rho' r U) = 0 \tag{5}$$

The radial and axial distances are normalized with respect to the outer tip radius of the compressor.

Upon substitution of the velocity, density, and pressure components of Eq. (1) into the momentum and continuity equations and neglecting terms of second order $\{0[\epsilon^2]\}$ or higher, we obtain

$$\bar{\rho}\bar{U}(\partial w/\partial x) = -\partial p/\partial r \tag{6}$$

$$\bar{\rho}\bar{U}(\partial v/\partial x) = -(1/r)\partial p/\partial \theta \tag{7}$$

$$\bar{\rho}\bar{U}(\partial u/\partial x) = -\partial p/\partial x \tag{8}$$

and

$$[\partial(rw)/\partial r] + (\partial v/\partial \theta) + r[(\bar{U}/\bar{\rho})(\partial \rho/\partial x) + (\partial u/\partial x)] = 0 \tag{9}$$

Eliminating p from any pair of Eqs. (6–8), we obtain three equations for the perturbation velocities satisfying the boundary condition that $u = v = w = 0$ at $x = -\infty$,

$$(\partial w/\partial\theta) - [\partial(rv)/\partial r] = 0 \tag{10}$$

$$(\partial w/\partial x) - (\partial u/\partial r) = 0 \tag{11}$$

$$[\partial(rv)/\partial x] - (\partial u/\partial\theta) = 0 \tag{12}$$

Equations (10–12) express the conditions of irrotational flow. Since the perturbation velocity field is irrotational, a potential function ϕ can be defined so that

$$u = \partial\phi/\partial x,\ v = (1/r)\partial\phi/\partial\theta, \text{ and } w = \partial\phi/\partial r \tag{13}$$

Substitution of Eq. (13) into the linearized continuity equations yields

$$\frac{\partial^2\phi}{\partial r^2} + \frac{1}{r}\frac{\partial\phi}{\partial r} + \frac{1}{r^2}\frac{\partial^2\phi}{\partial\theta^2} + \frac{\bar{U}}{\bar{p}}\frac{\partial\rho}{\partial x} + \frac{1}{r}\frac{\partial^2\phi}{\partial x^2} = 0 \tag{14}$$

Writing the density variation with x as $\partial\rho/\partial x = (\partial\rho/\partial p)\partial p/\partial x$ and combining with the isentropic flow relation, $\partial\rho/\partial p = 1/a^2$, where a is the local speed of sound yields $\partial\rho/\partial x = (1/a^2)\partial p/\partial x$. Substituting for $\partial p/\partial x$ from the linearized axial momentum equation, we obtain

$$\partial\rho/\partial x = -\bar{\rho}(\bar{U}/a^2)\partial u/\partial x = -\bar{\rho}(\bar{U}/a^2)\partial^2\phi/\partial x^2$$

Substitution of the previous result into Eq. (14) yields

$$(\partial^2\phi/\partial r^2) + (1/r)(\partial\phi/\partial r) + (1/r^2)(\partial^2\phi/\partial\theta^2) + (\partial^2\phi/\partial x_c^2) = 0 \tag{15}$$

where $x_c = x/(1 - M^2)^{1/2}$ and M is the local Mach number. Equation (15) is recognized to be Laplace's equation in circular cylindrical coordinates. Solving Eq. (15) with the appropriate boundary conditions yields the perturbation velocity potential function.

The boundary conditions for the upstream flowfield are

$$u = v = w = 0 \text{ at } x = -\infty \tag{16a}$$

$$w = 0 \text{ at } r = \gamma,\ r = 1 \tag{16b}$$

$$v = 0 \text{ at } \theta = 0 \tag{16c}$$

The γ is the normalized inner radius of the flow area and is equal to the hub-tip ratio of the compressor. Boundary condition in Eq. (16a) states that the perturbation velocities are zero at the distortion origin. Condition in Eq. (16b) states that the radial velocity is zero at the inner and outer wall of the annular flow region. Condition in Eq. (16c) states that the cross-flow velocity is zero at all points $\theta = 0$. This condition is satisfied for any symmetric distortion satisfying Eq. (1) with the points $\theta = 0$ and the axis of symmetry of the distortion coincident.

A general solution of Eq. (15) for $x_c \leq 0$ and satisfying the boundary condition is

$$\phi = \sum_m \sum_n A_{m,n} e^{\lambda_{m,n} x_c} \cos n\theta R(\lambda_{m,n} r) \tag{17}$$

where $A_{m,n}$ is a constant and $R(\lambda_{m,n}r)$ is a linear combination of Bessel functions of the first and second kind. The λ's are eigenvalues which satisfy the boundary condition of zero radial velocity at the inner and outer walls of the flow area and are tabulated in the Appendix. The subscripts m and n are the radial and circumferential harmonic numbers, respectively.

From the definition of the potential function [Eq. (13)] and the expression for the potential function [Eq. (17)] the perturbation velocity components are found to be

$$u = \sum_m \sum_n A_{m,n}\lambda_{m,n} e^{\lambda_{m,n} x_c} \cos n\theta R(\lambda_{m,n} r) \tag{18}$$

$$v = \frac{1}{r}\sum_m \sum_n - nA_{m,n} e^{\lambda_{m,n} x_c} \sin n\theta R(\lambda_{m,n} r) \tag{19}$$

$$w = \sum_m \sum_n A_{m,n} e^{\lambda_{m,n} x_c} \cos n\theta \frac{d}{dr}[R(\lambda_{m,n} r)] \tag{20}$$

The perturbation velocities vary exponentially with the axial distance parameter x_c. Therefore, the higher the Mach number, the shorter is the axial distance upstream of the compressor in which the major portion of the distortion attenuation takes place. The magnitude of the distortion attenuation is not affected by the Mach number in the first-order analysis.

Upon solving for the coefficients $A_{m,n}$, the velocity distribution in the upstream flowfield is solved for any inlet distortion given by Eq. (1). The coefficients are found from the boundary condition that the compressor imposes on the flowfield and the axial momentum equation.

Consider the conditions at the compressor. The static pressure at any point on the compressor face can be determined as a function of the axial velocity by subtracting the pressure rise across the compressor from the exit static pressure (assumed constant). If no distortion existed upstream, the upstream static pressure would be uniform throughout the flowfield and equal of $\bar{p}$. With the upstream distortion, the static pressure at the compressor face is modified by the perturbation pressure given by

$$p_{0_-} = -(\partial\Delta p/\partial U)\Delta U \tag{21}$$

where ΔU is the variation in the axial velocity at the compressor face from the undistorted velocity and is

$$\Delta U = \sum_n \epsilon_n \cos n\theta + u_{0_-}$$

where u_{0_-} is the axial velocity perturbation evaluated at $x = 0_-$ and is

$$u_{0_-} = \sum_m \sum_n A_{m,n}\lambda_{m,n} \cos n\theta R(\lambda_{m,n} r)$$

The term $\partial\Delta p/\partial U$ is the slope of the constant speed compressor characteristic expressed as static pressure rise vs axial velocity.

In addition to satisfying Eq. (21), the static pressure perturbation at any point at the compressor face must match that obtained from integration of the linearized axial momentum equation. Integration of Eq. (8) from $x = -\infty$ to $x = 0_-$ yields

$$p_{0_-} = -\bar{\rho}\bar{U}u_{0_-} \tag{22}$$

Equating Eqs. (21) and (22) yields

$$-(\partial\Delta p/\partial U)\Delta U = -\bar{\rho}\bar{U}u_{0_-} \tag{23}$$

Substituting for ΔU and u_{0_-} into Eq. (23) and equating coefficients of like terms, it can be shown that for every n,

$$\frac{\epsilon_n}{1 + (1/S_1)} = -\sum_m A_{m,n}\lambda_{m,n} R(\lambda_{m,n} r) \tag{24}$$

where,

$$S_1 = -(\partial\Delta p/\partial U)/\bar{\rho}\bar{U}$$

The parameter S_1 is the normalized slope of the static pressure rise vs axial velocity at constant rotational speed.

The coefficients $A_{m,n}$ are determined from Eq. (24) by employing the properties of orthogonal functions. Multiplying both sides of Eq. (24) by $rR(\lambda_{kn}r)$ and integrating over the radius yields

$$\int_\gamma^1 \frac{\epsilon_n R(\lambda_{k,n} r) r dr}{1 + 1/S_1} = -\sum_m A_{m,n}\lambda_{m,n} \int_\gamma^1 rR(\lambda_{m,n} r) R(\lambda_{k,n} r) dr \tag{25}$$

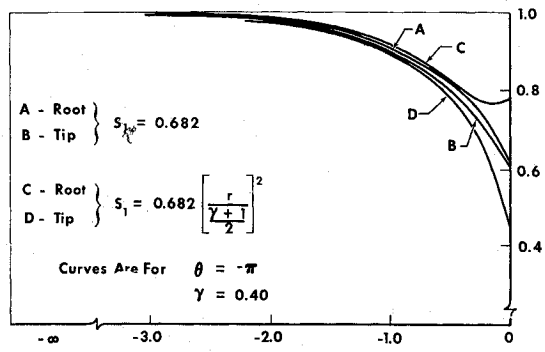

Fig. 2a) Normalized axial velocity distortion attenuation vs x—"long" compressor analysis—cosine wave distortion.

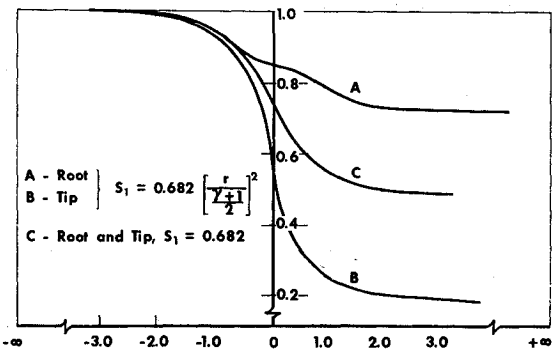

Fig. 2b) Normalized axial velocity distortion attenuation vs x—"short" compressor analysis—cosine wave distortion.

From the properties of orthogonal functions,

$$\int_\gamma^1 rR(\lambda_{m,n}r)R(\lambda_{k,n}r)dr = 0 \text{ for } k \neq m$$

Expanding Eq. (25), choosing any k and employing the previous yields

$$A_{m,n} = -\int_\gamma^1 \frac{\epsilon_n rR(\lambda_{m,n}r)dr}{1+1/S_1} \Big/ \lambda_{m,n}\int_r^1 rR^2(\lambda_{m,n}r)dr \quad (26)$$

In general, ϵ_n and S_1 are both functions of the radius. The integrals of Eq. (26) are most easily evaluated by numerical integration.

The three-dimensional velocity field is completely described upon evaluating Eq. (26) and substituting the result into the velocity equations. The static pressure at any point in the flowfield can then be evaluated using Eq. (22). The total pressure distortion remains unchanged in the upstream flowfield since no work has been done on the fluid.

When the analysis is repeated assuming conservation of radial velocity through the compressor ("short" compressor analysis), the upstream attenuation of the flow distortion is approximately one-half of that predicted by the "long" compressor analysis. Further attenuation of the flow distortion occurs downstream of the compressor giving an over-all attenuation approximately the same as that of the "long" compressor analysis.[6]

Analytical Results

Numerical solutions for the analysis were obtained. Two compressor designs were considered; one with a constant and one with a radially varying pressure rise vs axial velocity characteristic. The hub-tip ratio was set equal to 0.40 in both cases. A cosine wave ($n = 1$) distortion in axial velocity was set at $x = -\infty$. The cosine wave distortion coefficient ϵ_1 was chosen to produce a distortion that was uniform in the radial direction with a maximum amplitude of unity at $x = -\infty$. The Mach number was set equal to zero in the calculations.

The numerical solutions are presented graphically in Figs. 2–4. The calculated velocities are presented as normalized with respect to the maximum amplitude of the input perturbation.

Figure 2a presents the axial velocity distortion attenuation with respect to x. The axial parameter x is the axial distance from the compressor, normalized with respect to the compressor tip radius. Curves A and B represent the root and tip velocities, respectively, calculated with a constant S_1. Note that the total attenuation is the same but the rates of attenuation are different upstream of the compressor for the root and tip positions. This is an effect of the three-dimensional flow. Curves C and D represent the root and tip axial velocity attenuation for a varying S_1. The total attenuation is much greater at the tip than at the root and the attenuation at the root is not monotonic to the compressor face. The magnitude of the distortion at the root decreases steadily as the flow approaches the compressor face then increases slightly just upstream of the compressor. This is because the compressor causes a large attenuation of the axial velocity distortion at the tip and the fluid at the root is influenced by the large velocity (static pressure) change at the tip as well as the demands of the compressor at the root. Just upstream of the compressor, the demands of the compressor become stronger than the effect of the flow at the tip and the flow at the root is affected accordingly. The attenuation of the distortion is monotonic to the compressor face for a constant S_1 indicating that only large radial variations in the pressure-rise characteristic of the compressor or in the original distortion can produce axial velocity distortion attenuation profiles similar to that represented by curve C.

Figure 2b presents the normalized axial velocity distortion attenuation with respect to x calculated from an analysis of a "short" compressor. The upstream attenuation is similar, except in amplitude, to that calculated for a "long" compressor, and the downstream attenuation is predicted to be a mirror image of the upstream solution. Curves A and B are

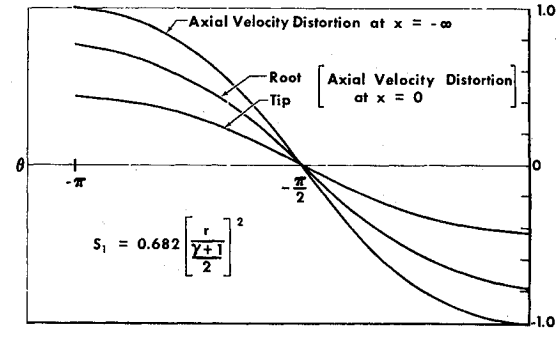

Fig. 3a) Normalized axial velocities vs θ—"long" compressor analysis—varying S_1—cosine wave distortion.

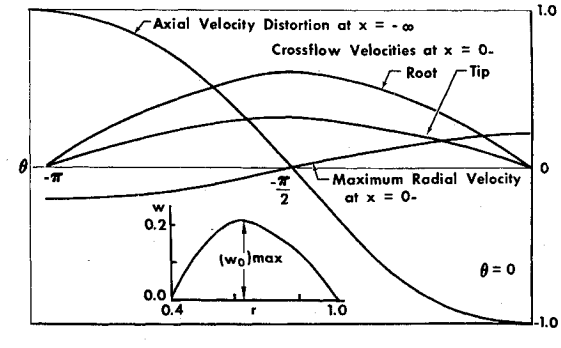

Fig. 3b) Normalized circumferential and radial velocities vs θ—varying S_1—cosine wave distortion.

the root and tip distortion attenuation curves calculated for radially varying S_1. Curve C represents the distortion attenuation when S_1 is assumed constant.

Figures 3a and 3b present the normalized distortion velocities vs θ calculated at $x = 0_-$ assuming a constant exit static pressure profile and a radially varying S_1. Because of the circumferential symmetry of the flowfield for a cosine wave distortion only the negative half of the circumferential coordinate is presented. The axial velocity distortion at the root has attenuated to about 78% of the input distortion and the remaining distortion at the tip is 45% of the input distortion. The axial attenuation rates are shown by curves C and D of Fig. 2a.

The normalized cross-flow and radial velocity components generated in the upstream flowfield are shown vs θ in Fig. 3b. The maximum cross-flow velocity occurs at the root of the flow area, and at the compressor face is equal to 60% of the axial velocity distortion at its origin. The cross flow at the tip section is approximately 35% of the input distortion. The generated radial velocity varies with the radius and must be zero at the annulus walls. The maximum radial velocity at the compressor face is plotted vs θ and is shown to be 20% of the input axial velocity distortion. The radial variation of w at $\theta = 0$ is also shown and the maximum w is located at a radius less than the mean radius of the annulus.

Figure 4 graphically illustrates the effect of different inlet Mach numbers on the distortion attenuation. It is apparent that when M is less than about 0.3 the changes in the rate of attenuation with x compared to an M of zero are small. A higher Mach number only changes the axial distance in which a major portion of the distortion attenuation occurs and not the magnitude of the distortion attenuation at the compressor face.

Experimental Apparatus and Tests

An apparatus was designed and constructed to examine distorted three-dimensional flowfields upstream of a low hub-tip ratio axial flow compressor. Basic requirements of the test apparatus included the generation of an inlet velocity or total pressure distortion far upstream of a low hub-tip ratio axial compressor and a complete three-dimensional survey of the velocities and pressures as the flow approached the compressor.

A schematic of the test apparatus is shown in Fig. 5. The test compressor is a single-stage Joy axivane fan. The fan was designed for an axial flow inlet and exit and has no inlet guide vanes. The fan has 10 rotor blades and was modified by adding an additional stator between each of the eight stators installed by the manufacturer, allowing for better control of the flow at the fan exit. The ratio of the stage length to the blade height is 2.1 representing a relatively "long" compressor stage.

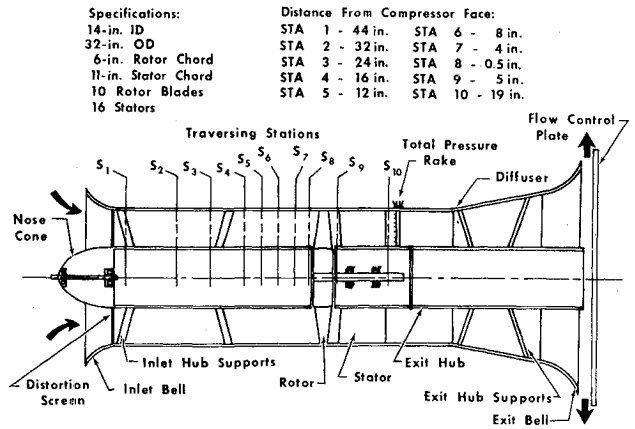

Fig. 5 Test apparatus schematic.

The inlet test section and the compressor were instrumented to obtain a survey of the three-dimensional flow. To obtain a good survey of the flowfield, 10 axial measuring stations were selected as shown in Fig. 5. The measuring stations were spaced closer together near the compressor face because the results of Plourde and Stenning indicated that a large percentage of the flow redistribution occurs in that region. Wall static pressure taps were placed at the inner and outer walls of the flow area at each of the axial stations. To obtain the pressures and velocities in the test section a five-hole traversing probe was used. The circumferential survey was obtained by changing the circumferential position of the inlet distortion screen supported by the nose cone.

A suitable compressor speed was determined for the testing and the undistorted static pressure rise vs axial velocity compressor characteristic was generated as shown by the solid curve in Fig. 6. The normalized static pressure-rise across the compressor is plotted vs the normalized axial velocity. The solid curve was generated from data observed at the mean radial position of the compressor blading. Root and tip behavior was similar with slightly different slopes. The small variation from root to tip was accounted for in the analysis.

A distortion test was initiated using a cosine wave distortion profile far upstream. It was found difficult to generate an inlet distortion profile that exactly represented a cosine wave. The screen was constructed by laminating several small screens of 20° segments until the desired shape was approximated. The mean axial velocity at the inlet for this test was 73 fps with a ±25 fps distortion superposed on the main flow. The static pressures at the compressor face and exit are presented in Fig. 7. The static pressure was essentially constant at the compressor exit. A complete velocity survey was ob-

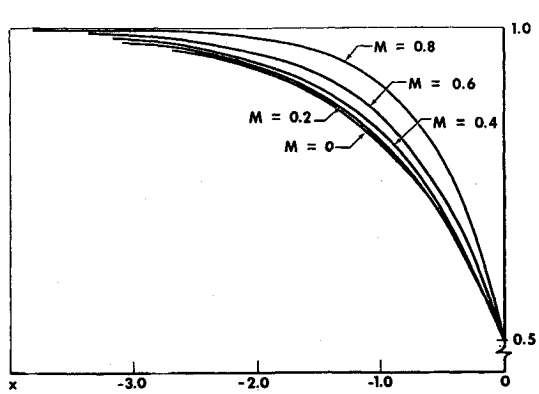

Fig. 4 Normalized axial velocity distortion vs x for different inlet Mach numbers.

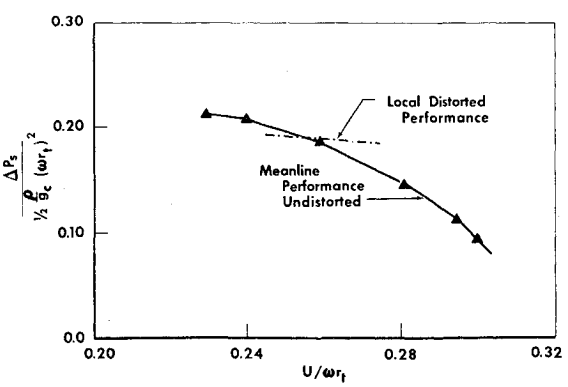

Fig. 6 Static pressure rise vs axial velocity compressor characteristic.

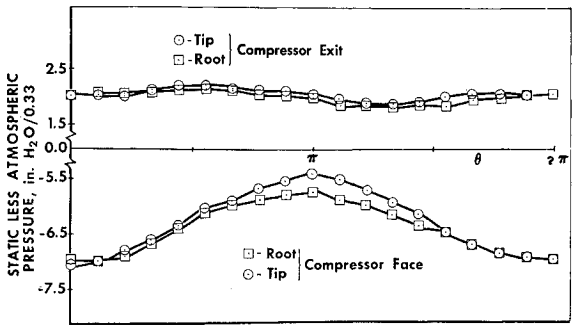

Fig. 7 Inner and outer wall static pressures at compressor face and exit—cosine wave distortion.

tained upstream of the compressor and the axial and circumferential velocity components are shown in Figs. 8a–8d.

Comparison of Experiment and Theory

Two things must be known to apply the analysis: 1) the shape and magnitude of the input distortion and 2) the parameter S_1, obtained from the pressure-rise characteristic of the compressor.

The shape and magnitude of the input distortion is produced by the Fourier cosine series,

$$\sum_n \epsilon_n \cos n\theta$$

The accuracy of the fit is determined by the number of terms included in the series.

The parameter S_1 is a function of the slope of the pressure-rise characteristic of the compressor. It was noted, for the particular compressor used, that the local slope of the compressor characteristic for distorted operation was approximately $\frac{1}{3}$ the local slope during undistorted operation. This compressor had an unusually large value of the corrected frequency parameter, and in consequence unsteady flow effects were important. These effects partially explain the difference between the distorted and undistorted local slopes. A more detailed discussion of the unsteady effects can be found in Ref. 6.

The value of $(S_1)_{\text{distorted}}$ was determined from the following relationships:

The Bernoulli equation for any point in the upstream flowfield is

$$P_t' = p_s' + (\rho'/2g_c)U^2 \tag{27}$$

where the subscripts t and s signify total and static conditions, respectively. Differentiating Eq. (27) yields

$$dU = g_c[d(p_t - p_s)/\bar{p}\bar{U}] \tag{28}$$

The pressure-rise parameter can be written,

$$S_1 = -(g_c/\bar{p}\bar{U})\partial\Delta p/\partial U \tag{29}$$

where Δp is the local static pressure rise across the compressor. Combining Eqs. (28) and (29) yields

$$S_1 = -\partial\Delta p/\partial(p_t - p_s)_{0-} \tag{30}$$

The term $(p_t - p_s)_{0-}$ is the difference between the total and static pressures at the compressor face.

The slope of a line passing through the data on a plot of Δp vs $(p_t - p_s)_{0-}$ for different circumferential positions from the high-energy region to the low-energy region of the distortion is the value of $(S_1)_{\text{distorted}}$. The dashed curve in Fig. 6 shows the local variations in static pressure rise around the circumference of the compressor. Using this procedure, the pressure-rise parameter was found to be $(S_1)_{\text{distorted}} = 0.832r + 0.215$.

Comparisons of the theoretical predictions and the experimental results are presented in Figs. 8a–8d. The experimental axial velocities are plotted about their respective mean axial velocities, hence, only the velocity distortions are presented. It was necessary to present the velocities in this manner because the boundary-layer buildup along the inner and outer walls of the flow area caused the mean axial velocity to change as the flow approached the compressor face. The

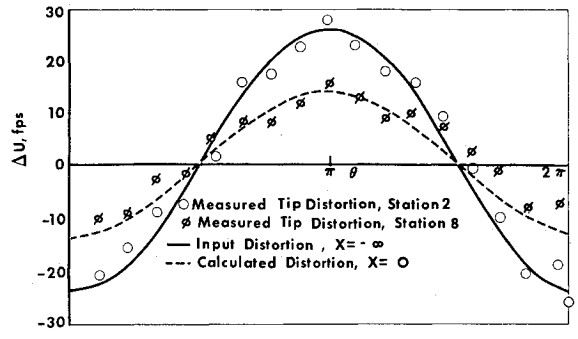

Fig. 8a) Measured and theoretical axial velocity distortion vs θ—cosine wave distortion—stations 2 and 8, tip.

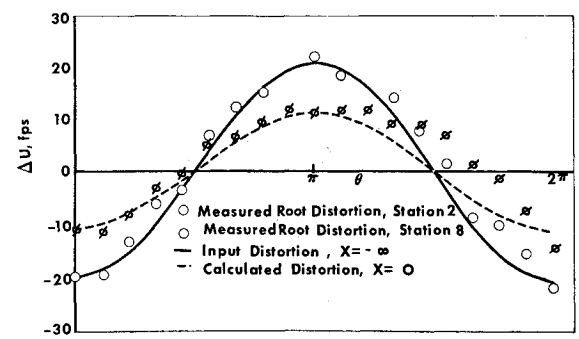

Fig. 8b) Measured and theoretical axial velocity distortion vs θ—cosine wave distortion—stations 2 and 8, root.

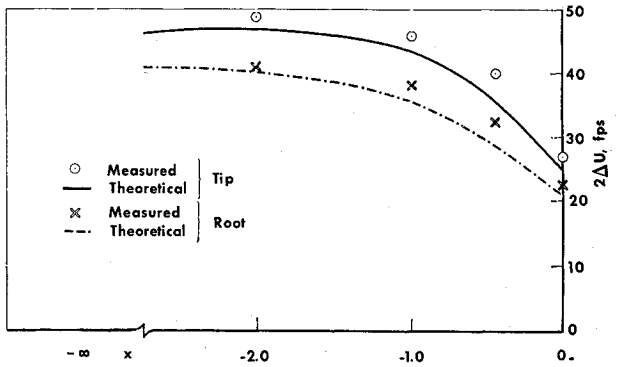

Fig. 8c) Measured and theoretical axial velocity distortion vs x—cosine wave distortion—root and tip.

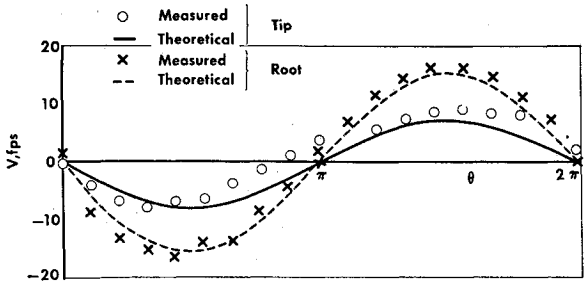

Fig. 8d) Measured and theoretical cross-flow velocities at root and tip at station 8—cosine wave distortion.

theoretical predictions are easily compared with the data presented in this form since the analysis only predicts the distorted velocity field which is assumed to be superposed on a mean axial velocity.

The measured and predicted velocity profiles for the cosine wave distortion are presented in Fig. 8. The input distortion was approximated with a single cosine term. Four radial harmonics were included in the double summation when the perturbation velocities were calculated. Because the cosine distortion was difficult to generate, a 360° circumferential survey was obtained to check the circumferential symmetry.

Figures 8a and 8b present the measured and predicted axial velocity distortion vs θ both far upstream and at the compressor face for the cosine wave distortion. Figure 8a is for the tip of the flow area and Fig. 8b is for the root of the flow area. The prediction of the distortion attenuation is quite good from 0° to 180° but deviates from the data $\theta > 180°$. Two explanations for the discrepancy are 1) the distortion is not perfectly symmetric and 2) the input distortion was chosen to fit the data from 0° to 180° rather than over the entire circumference.

Figure 8c presents the measured and predicted axial velocity distortion vs x from the root and tip of the flow area. The rate of attenuation is predicted well but the predicted magnitude of the distortion is less than that observed. This is mainly because the approximation to the distortion was chosen for the best fit for all θ between 0° and 180° and not just for the maximum amplitude of the distortion.

The measured and predicted cross-flow velocities at the root and tip radii at the compressor face are shown in Fig. 8d to be in good agreement. Both the predicted distribution and magnitude of the cross-flow velocities match the experimental results.

An equally satisfactory comparison between theory and experiment was obtained for a test using a circumferential square wave distortion. Details of this test are given in Ref. 6.

Conclusions

This paper has attempted to describe the flowfield upstream of a low hub-tip ratio compressor operating with a total pressure distortion originating far upstream. A clear distinction has been found to exist between compressors which are sufficiently long to suppress radial velocities induced upstream, and compressors for which radial velocities are conserved in passing through the compressor. For "long" compressors the static pressure is essentially uniform after the last stator row. For "short" compressors considerable nonuniformity in static pressure can exist downstream. Although the test results gave good agreement with the "long" compressor analysis, it is not clear whether this would be true of all jet engine compressors, and single-stage fans of high aspect ratio might depart considerably from the "long" compressor assumptions.

For the fan tested, the analysis gave a good prediction of the axial, circumferential, and radial velocities induced ahead of the compressor when the appropriate local slope was used. This fan had an unusually large value of the corrected frequency parameter, and in consequence unsteady flow effects were important. For jet engine compressors, the undistorted slope should give a good prediction of the induced flowfield.

Appendix

The eigenvalues $\lambda_{m,n}$ are essential to the evaluation of the potential function in the cylindrical analysis. Dunham[1] has determined a set of eigenvalues corresponding to an annular flow area of hub-tip ratio 0.40. For the experimental part of this study an axial flow compressor of hub-tip ratio 0.437 was used. Eigenvalues corresponding to this hub-tip ratio were required to compare the theoretical predictions with the experimental data and are presented in Table 1.

Table 1 Eigenvalues corresponding to $\gamma = 0.437$

n/m	0	1	2	3
0	(0)	5.719	11.237	16.793
1	1.423	5.945	11.343	16.863
3	4.062	7.578	12.179	17.414
5	6.389	10.102	13.774	18.486
7	8.573	12.753	16.003	20.046

References

[1] Dunham, J., "Non-Axisymmetric Flows in Axial Compressors," Ph.D. thesis, 1962, University of Cambridge, Pembroke College, Cambridge, England.

[2] Pearson, H. and McKenzie, A. B., "Wakes in Axial Compressors," *Journal of the Royal Aeronauical Society*, Vol. 63, No. 583, 1959, p. 415.

[3] Plourde, G. A. and Stenning, A. H., "The Attenuation of Circumferential Inlet Distortion In Multi-Stage Axial Compressors," *Journal of Aircraft*, Vol. 5, No. 3, May–June, 1968.

[4] Robbins, W. H. and Glaser, F., "Experimental Investigations of the Effect of Circumferential Inlet Flow Distortion on the Performance of a Five-Stage Axial-Flow Research Compressor with Transonic Rotors in all Stages," RM-E57J17, March 1968, NASA.

[5] Dunham, J., "Non-Axisymmetric Flows in Axial Compressors," Mechanical Engineering Science Monograph No. 3, 1965, Institution of Mechanical Engineers.

[6] Callahan, G. M., "Attenuation of Inlet Flow Distortion Upstream of Axial Flow Compressors," Ph.D. thesis, 1968, Lehigh University.